

NANO EXPRESS

Open Access



Facile Fabrication of BiF₃: Ln (Ln = Gd, Yb, Er)@PVP Nanoparticles for High-Efficiency Computed Tomography Imaging

Jun Xie^{1†}, Zonglang Zhou^{3†}, Sihan Ma², Xian Luo¹, Jiajing Liu¹, Shengyu Wang¹, Yuqiang Chen^{1,3*}, Jianghua Yan^{1*} and Fanghong Luo^{1*}

Abstract

X-ray computed tomography (CT) has been widely used in clinical practice, and contrast agents such as Iohexol are often used to enhance the contrast of CT imaging between normal and diseased tissue. However, such contrast agents can have some toxicity. Thus, new CT contrast agents are urgently needed. Owing to the high atomic number ($Z = 83$), low cost, good biological safety, and great X-ray attenuation property ($5.74 \text{ cm}^2 \text{ kg}^{-1}$ at 100 keV), bismuth has gained great interest from researchers in the field of nano-sized CT contrast agents. Here, we synthesized BiF₃: Ln@PVP nanoparticles (NPs) with an average particle size of about 380 nm. After coating them with polyvinylpyrrolidone (PVP), the BiF₃: Ln@PVP NPs possessed good stability and great biocompatibility. Meanwhile, compared with the clinical contrast agent Iohexol, BiF₃: Ln@PVP NPs showed superior in vitro CT imaging contrast. Subsequently, after in situ injection with BiF₃: Ln@PVP NPs, the CT value of the tumor site after the injection was significantly higher than that before the injection (the CT value of the pre-injection and post-injection was 48.9 HU and 194.58 HU, respectively). The morphology of the gastrointestinal (GI) tract can be clearly observed over time after oral administration of BiF₃: Ln@PVP NPs. Finally, the BiF₃: Ln@PVP NPs were completely discharged from the GI tract of mice within 48 h of oral administration with no obvious damage to the GI tract. In summary, our easily synthesized BiF₃: Ln@PVP NPs can be used as a potential clinical contrast agent and may have broad application prospects in CT imaging.

Keywords: Facile synthesized strategy, BiF₃: Ln@PVP nanoparticles, Contrast agents, Computed tomography, Gastrointestinal tract imaging

Introduction

X-ray computed tomography (CT) can image internal tissues and organs in a cross-sectional way with high resolution and low price [1, 2]. Thus, it is an important means to diagnose respiratory diseases, digestive diseases, and urinary system diseases [3–8]. However, CT sometimes has low contrast between diseased tissues and normal tissues. Thus, contrast agents such as Iohexol are widely

used in clinical practice to specifically enhance the X-ray attenuation of diseased tissues. However, the clinical contrast agents are often used in large doses due to the low sensitivity of CT detectors [9]. In addition, commercial iodine-based contrast agents have an extremely fast metabolism in the body and severe side effects, including cardiac events and nephrotoxicity; these issues limit their clinical use and should be solved urgently [10–15].

Nanomaterials have shown broad application prospects in environmental remediation, photovoltaic applications, catalysts, etc. [16–21]. For instance, Balati et al. [22] have synthesized a heterostructured photocatalyst (HBTiO₂/RBIHM-MoS₂) using pulsed laser ablation in liquid (PLAL) followed by microwave irradiation.

*Correspondence: chenyaq707@163.com; jhyang@xmu.edu.cn; luofanghong@xmu.edu.cn

[†]Jun Xie and Zonglang Zhou contributed equally to this work

¹Cancer Research Center, Medical College, Xiamen University, Xiamen 361102, China

Full list of author information is available at the end of the article

Nanomaterials have also been widely used in medicine, including imaging and treatment.

Gold (Au), tantalum (Ta), platinum (Pt), and other elements with high X-ray attenuation have gained the interest of researchers, and nanomaterials synthesized from these elements have been well-researched as potential contrast agents for CT imaging [1, 12–15, 23, 24]. However, their high price and uncertain biosafety limits their further use. Bismuth (Bi) is well-known as a biosafe element with low cost. It has been used in clinical practice and plays a critical role in combination therapy for *Helicobacter pylori* and other diseases, including chronic liver disease as well as gastric and duodenal ulcers. It has great biological safety and tolerance during treatment [7, 25]. Also, Bi has been used in the preparation of nanoscale contrast agents such as HA-BiO NPs, Bi₂S₃, BION, and Bi₂Te₃ because of its high atomic number ($Z=83$) and excellent X-ray attenuation capacity ($5.74 \text{ cm}^2 \text{ kg}^{-1}$ at 100 keV) [26–29].

For instance, Mohsen Mahvi et al. synthesized Bi₂Te₃ nanoflakes via a microwave-assisted polyol process that showed a better X-ray attenuation coefficient than commercial Iohexol [29]. Thus, Bi is a promising element for constructing high-performance CT contrast agents. However, the preparation of Bi-based nanocontrast agents is complicated [30, 31].

Here, we combined Bi with lanthanides (Gd, Yb, Er) via a facile and low-cost protocol to fabricate BiF₃: Ln@PVP nanoparticles (NPs). We then investigated its potential for generating contrast for CT imaging. After coating the samples with PVP, BiF₃: Ln@PVP NPs showed good stability and low biological toxicity. These samples exhibit better X-ray attenuation than commercial Iohexol in vitro, have good in vivo contrast, and offer great gastrointestinal (GI) tract CT imaging. Importantly, after 48 h of oral administration of BiF₃: Ln@PVP, the nanoparticles were completely excreted from the body showing no obvious damage to vital organs such as the liver and the kidneys. We believe that our work may provide a new theoretical basis for the clinical use of nanoscale CT contrast agents.

Methods

All experimental protocols including animal experiments were approved by the ethics committee of Xiamen University in Fujian Province, China.

Materials and Reagents

Bismuth nitrate pentahydrate (Bi(NO₃)₃·5H₂O, ≥ 99.99%), ammonium fluoride (NH₄F, ≥ 99.99%), ytterbium nitrate hexahydrate (Yb(NO₃)₃·6H₂O, ≥ 99.9%), erbium nitrate hexahydrate (Er(NO₃)₃·6H₂O, ≥ 99.9%), gadolinium nitrate hexahydrate (Gd(NO₃)₃·6H₂O, ≥ 99.9%),

polyvinylpyrrolidone (PVP, ≥ 99.0%), and Iohexol (≥ 99.0%) were bought from Aladdin Reagents (Shanghai, China). The live-dead cell staining kit and cell counting kit-8 (CCK-8) were bought from Yeasen (Shanghai, China). The RPMI medium 1640, penicillin, streptomycin, and fetal bovine serum (FBS) were purchased from Gibco (New York, USA).

Fabrication of BiF₃: Ln@PVP NPs

The BiF₃: Ln@PVP NPs were synthesized via a hydrothermal approach. In detail, 1 mmol Ln(NO₃)₃ (Ln = Yb, Er and Gd), and 1 mmol Bi(NO₃)₃ were dissolved into a 35-mL solution including 5-mL deionized water (DI) and 30-mL ethylene glycol to form a transparent solution A. This was then mixed with 0.5 g PVP ($M_w = 10,000$) and stirred at room temperature for 10 min. NH₄F (20 mmol) was dissolved into 10-mL DI to form solution B. Solution B was then poured into solution A, and a white mixture solution C was formed after stirring for 20 min. Solution C was then put into a 50-mL autoclave and heated to 180 °C for 24 h. The temperature naturally dropped to room temperature after 24 h. Finally, the samples were centrifuged (8000 rpm, 3 min) and rinsed by DI and alcohol to wash away the un-reacted substances. The last samples were gathered by freeze-drying.

Characterization of BiF₃: Ln@PVP NPs

The morphology of BiF₃: Ln@PVP NPs was detected by transmission electron microscopy (TEM, TECNAI G20 F30 TWIN, Oxford) with an operating voltage of 300 kV. The composition of the nanoparticles was analyzed by energy dispersive spectrum (EDS) in TEM including map analysis. The Fourier transform infrared spectroscopy (FTIR, Thermo Scientific Nicolet iN10 MX spectrometer, USA) was used to distinguish the functional groups of the samples. The crystal structures and phase feature of the BiF₃: Ln@PVP NPs used powder X-ray diffraction (XRD, D8 Advance) with Cu K α radiation under 40 kV and 40 mA conditions. The size distribution of the nanoparticles dispersed in DI and PBS (pH 7.4) was investigated by dynamic light scattering (DLS, Brookhaven Instruments-Omni, USA).

Cell Line and Cell Culture: HepG2 cells were from the Cell Bank of the Chinese Academy of Sciences (Shanghai, China). Cells were cultured in RPMI medium 1640 containing 10% fetal bovine serum (FBS) and 1% penicillin-streptomycin under 37 °C and 5% CO₂ conditions. The culture media was replaced every other day.

Cytocompatibility of BiF₃: Ln@PVP NPs In Vitro

The cytocompatibility of BiF₃: Ln@PVP NPs in vitro was estimated by a live-dead assay and the CCK-8 assay. In detail, the HepG2 cells were collected and seeded in

confocal dishes at 5.0×10^5 . The cells were then cultured overnight. The BiF₃: Ln@PVP NP suspensions were next added to the cells at different concentrations (100, 200, and 400 µg/mL) and set as the experimental groups. Meanwhile, medium without nanoparticles was added and set as the control group. Subsequently, both the experimental groups and the control group were cultured for 24 h. After 24 h, we gently removed the original medium and the live-dead assay was then performed according to the protocol provided by the manufacturer. Briefly, the living cells were labeled via Calcein-AM, while the dead cells were stained by propidium iodide (PI); cells were then observed under a confocal microscope (Nikon, Japan).

A CCK-8 assay was performed to further determine the cytotoxicity of BiF₃: Ln@PVP NPs in vitro. In detail, the HepG2 cells were collected and seeded in a 96-well plate with 3000 cells per well and cultured in an incubator overnight. Different concentrations of BiF₃: Ln@PVP NP (0, 25, 50, 100, 200, and 400 µg/mL) were mixed with the cells and cultured for 24 h. The CCK-8 reagent (10 µL) was added into each well and incubated for 2 h at 37 °C conditions. Later, the OD values of each well were measured at 450 nm by a SPECTRA max Microplate Reader (model 680, Bio-Rad, Tokyo, Japan), and the cell viability of each concentration was calculated according to the formula provided by the manufacturer. These experiments were repeated three times.

Animals

Female BALB/c nude mice (4- to 6-week-old) were obtained from Xiamen University Laboratory Animal Center (Xiamen, China). The mice were reared in a sterile environment and maintained for a 12-h light/dark cycle. The animals were injected with HepG2 cells (1.0×10^7 /mL) subcutaneously to induce tumor formation. All of the animal experiments in this work were conducted according to the protocol approved by the Animal Care and Use Committee of Xiamen University.

Biocompatibility of BiF₃: Ln@PVP NPs In Vivo

Histological analysis was used to observe the biocompatibility of BiF₃: Ln@PVP NPs in vivo. The experimental group mice were injected with a BiF₃: Ln@PVP NP suspension at 200 mg/kg through the tail vein; control mice were intravenously injected with the same volume of PBS. After 24 h, the major organs including hearts, livers, spleens, lungs, kidneys, and brains were immediately removed after the mice were sacrificed. All of the organs were fixed with 4% paraformaldehyde fixative for 12 h and then embedded in paraffin and sliced. Finally, hematoxylin–eosin (H&E) staining was performed. The morphology of the organs was evaluated and captured

by an upright fluorescence microscope (Leica DM2700 P, Germany).

CT Performance of BiF₃: Ln@PVP NPs In Vitro and In Vivo

To study the application of BiF₃: Ln@PVP NPs in vitro CT imaging, BiF₃: Ln@PVP NP and Iohexol suspensions were prepared and diluted to 0, 0.625, 1.25, 2.5, 5.0, 10.0, and 20.0 mg/mL and removed into 0.3-mL Eppendorf tubes. The CT images and the corresponding CT values of BiF₃: Ln@PVP NP and Iohexol suspensions were obtained and recorded by an X-ray CT instrument (Siemens) with an operating voltage of 50 kV and 80 kV, respectively. Next, the CT imaging ability of BiF₃: Ln@PVP NPs in vivo was studied; The BiF₃: Ln@PVP NP suspension was intratumorally injected into the tumor-bearing nude mice at 200 mg/kg (100 µL). Subsequently, the mice were anesthetized and the X-ray CT machine (Siemens, 80 kV, 88 µA) was used to capture CT images before and after administration of BiF₃: Ln@PVP.

CT Performance of BiF₃: Ln@PVP NPs in GI Tract and Histological Analysis

To further explore the value of BiF₃: Ln@PVP NPs in CT imaging, the mice were fasted overnight and orally administrated a BiF₃: Ln@PVP NP suspension (300 µL, 20 mg/mL) through a gastric tube. The mice were then intraperitoneally anesthetized with chloral hydrate. Next, GI images at different intervals (0, 15 min, 30 min, 120 min, 6 h, 12 h, 24 h, and 48 h) were captured at 80 kV. Finally, 3D models of the mice were reconstructed via the CT machine. The mice were then sacrificed and the stomachs, small intestines and large intestines were removed and fixed with 4% paraformaldehyde for 12 h. They were then embedded in paraffin and sectioned before H&E staining to evaluate the gastrointestinal toxicity of BiF₃: Ln@PVP NPs.

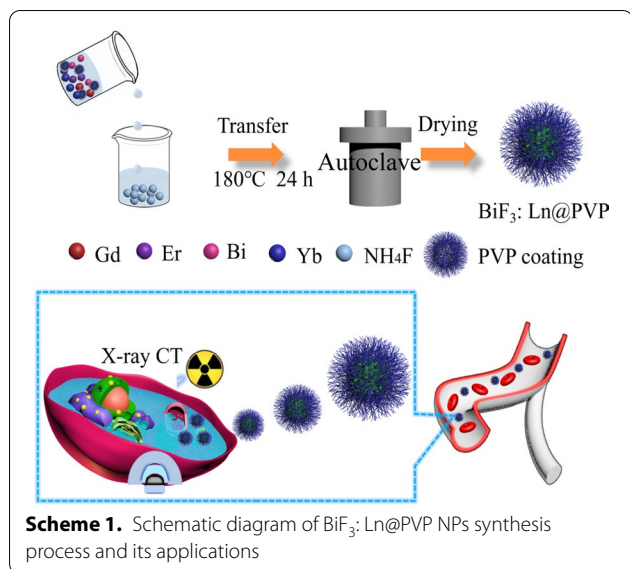
Statistical Analysis

Data were analyzed using one-way ANOVA; a *P* value < 0.05 was considered statistically significant in all analyses (95% confidence level).

Results and Discussion

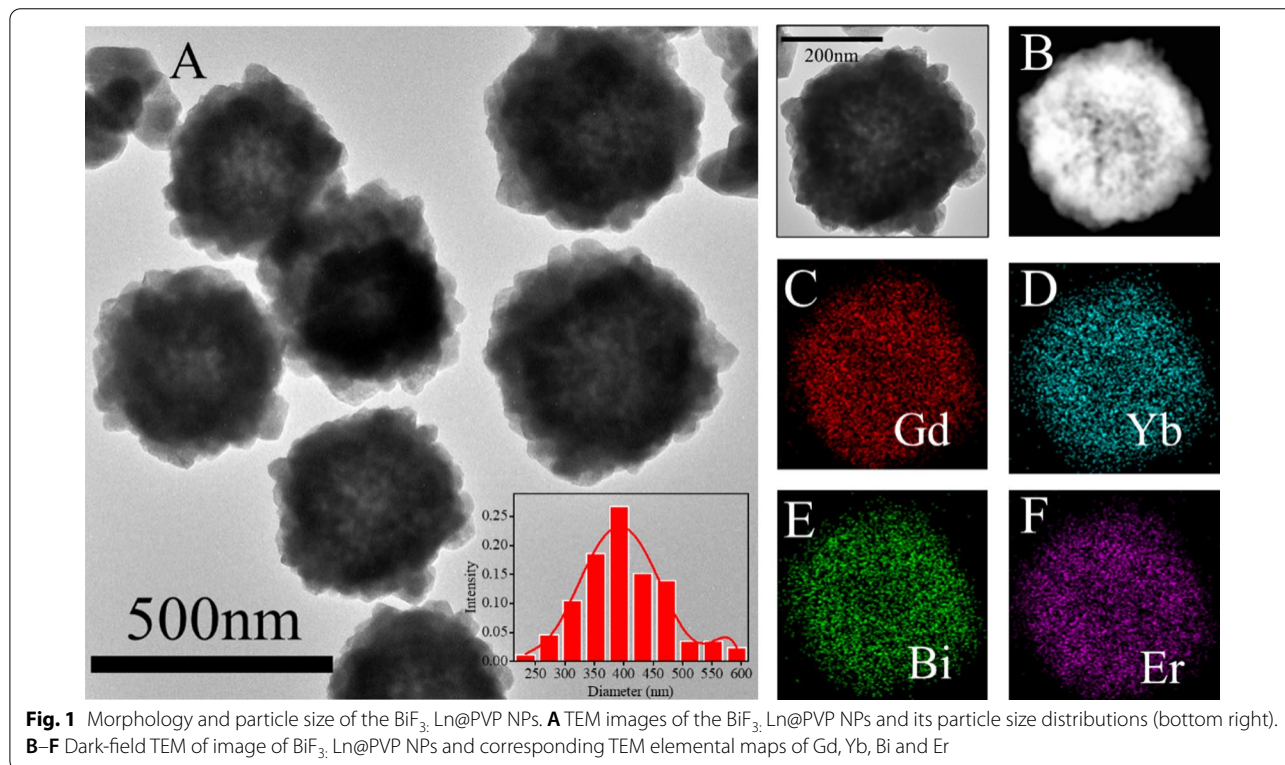
Fabrication and Physicochemical Properties of the BiF₃: Ln@PVP NPs

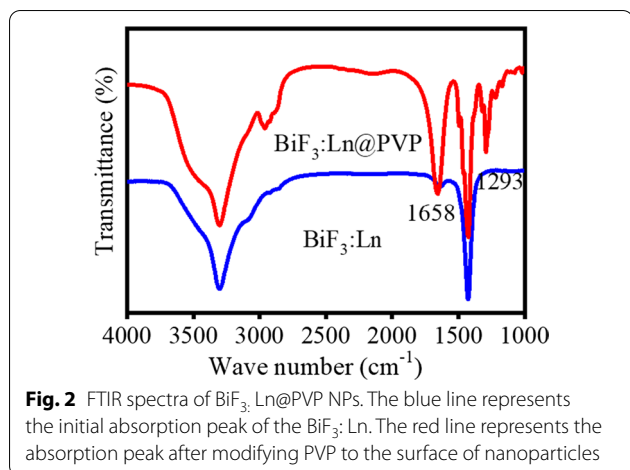
First, the BiF₃: Ln@PVP NPs were prepared through a hydrothermal reaction (Scheme 1). Figure 1A shows the morphology of the BiF₃: Ln@PVP NPs by TEM. The BiF₃: Ln@PVP NPs have a uniform and spherical structure. The mean size of the BiF₃: Ln@PVP NPs is about 380 nm and is evenly dispersed. The insert figure shows that the nanoparticles have a relatively narrow particle size distribution (bottom right). The composition of BiF₃: Ln@



PVP NPs were analyzed by EDS after evaluating the morphology of the BiF₃:Ln@PVP NPs. Figure 1B–F shows a dark-field image of BiF₃:Ln@PVP NPs taken before elemental analysis. The results show that our nanoparticles are mainly composed of Gd, Yb, Er, and Bi elements, indicating that the BiF₃:Ln@PVP NPs were successfully synthesized.

PVP is an effective stabilizer to improve the biocompatibility and stability of nanomaterials [32]. Therefore, we modified our nanoparticles with PVP as previously reported [33]. FTIR spectra were used to determine whether the PVP was successfully coated on the surface of the nanoparticles (Fig. 2). There were C=O group strong absorption peaks and C–N group peaks at 1658 and 1293 cm⁻¹, respectively. These were from PVP indicating that the coating of PVP on the surface of the nanoparticles was complete [34]. The XRD pattern of the BiF₃:Ln@PVP NPs are shown in Fig. 3. Figure 3A shows that all peaks are well-matched with standard card BiF₃:Ln data (PDF 74-0144) further demonstrating that the BiF₃:Ln@PVP NPs were successfully prepared. The atomic parameters of the BiF₃ structure can be used as the initial parameters in the standard cif card via Diamond software. The standard structure yielded PDF 74-0144, $a = b = c = 5.865 \text{ \AA}$, $V = 201.75(3) \text{ \AA}^3$, and density (ρ) = 8.755. The BiF₃ crystal structure viewed from the C-axis has layers stacked in the direction perpendicular to the A-axis (Fig. 4B), and the view of a single structure from the A-axis shows Bi is in the center of the atom (Fig. 4C). These results indicate that BiF₃:Ln@PVP NPs have a good crystal structure, and the surface coating only slightly influences the crystal structure of BiF₃:Ln@PVP NPs.



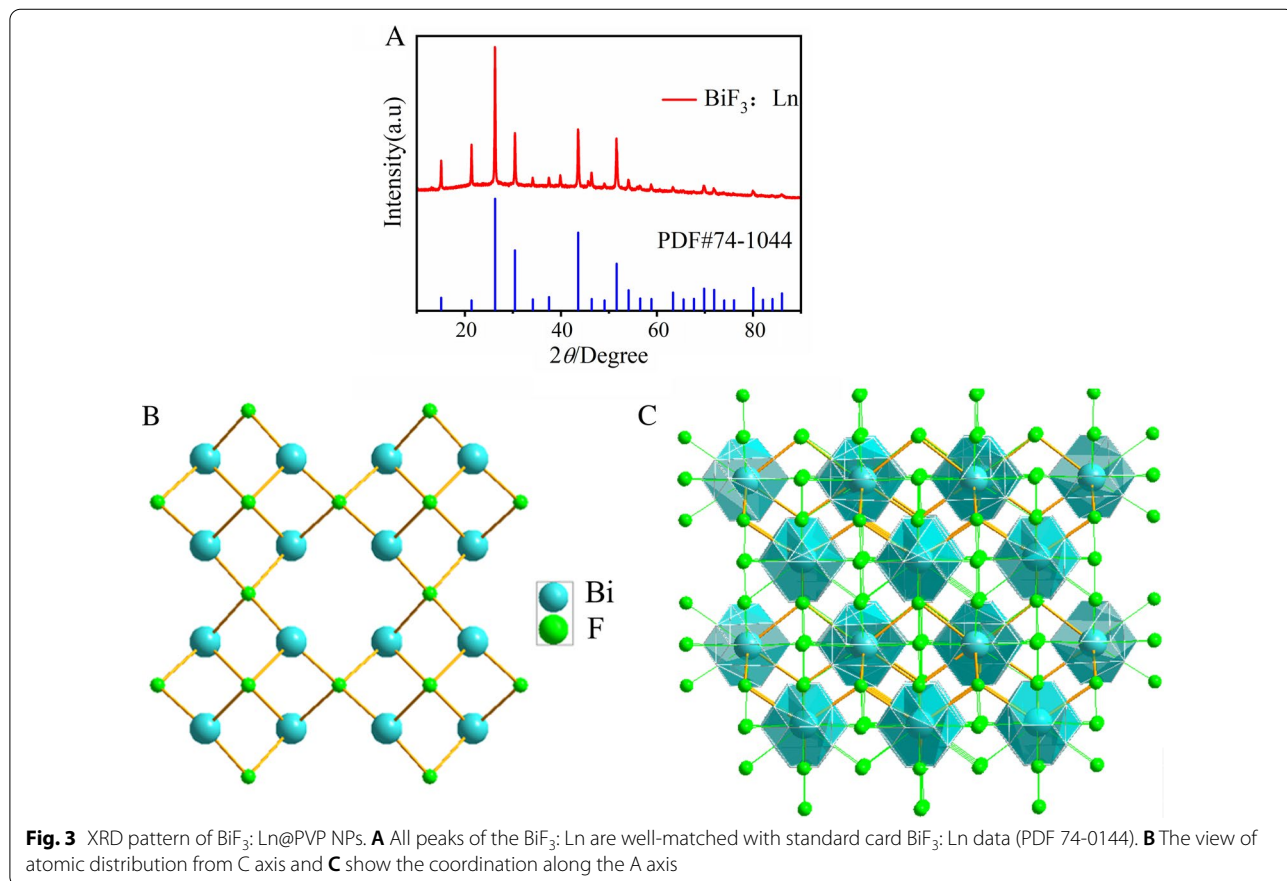


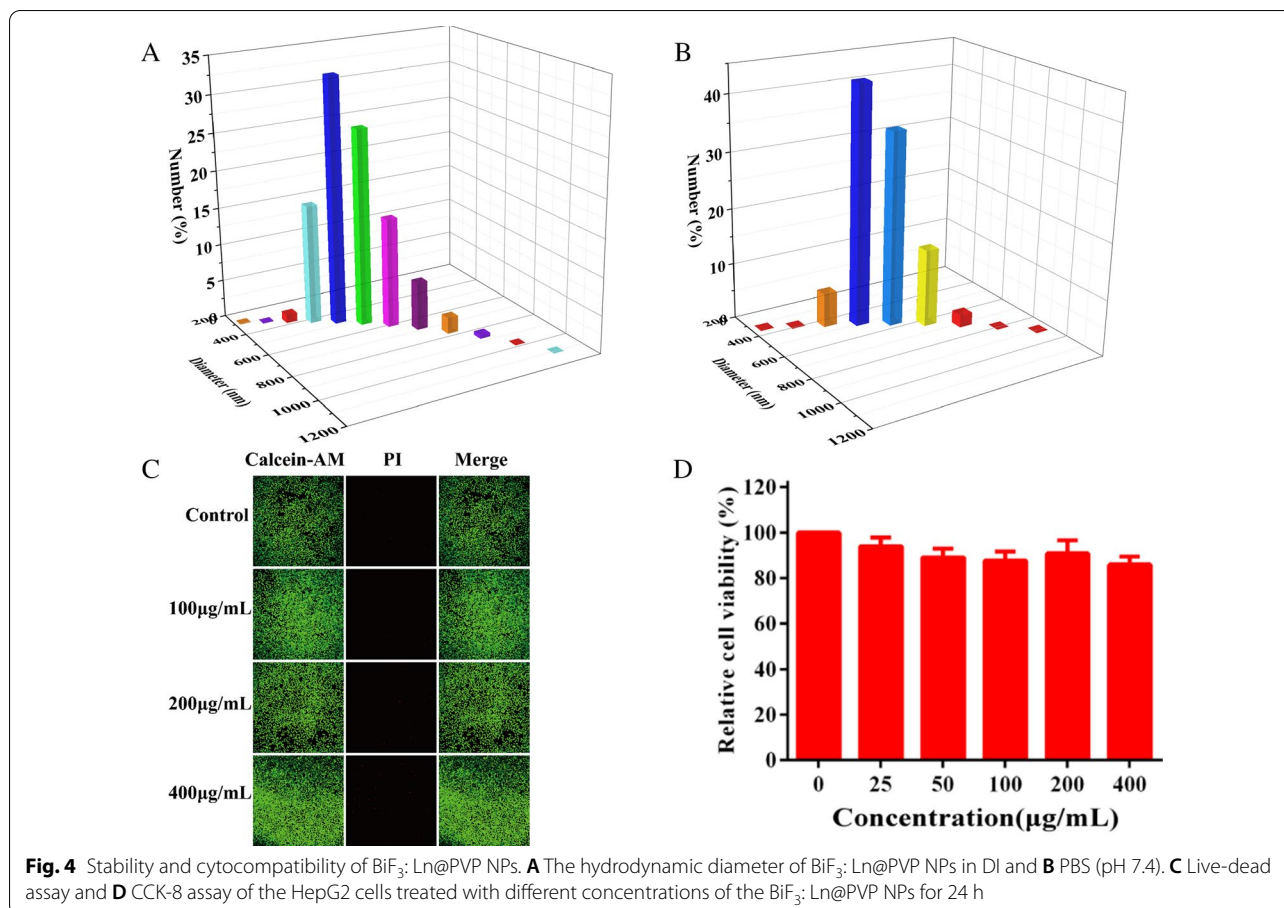
Stability and Cytocompatibility of BiF₃:Ln@PVP NPs

Since the dispersion size of nanoparticles can affect the interaction with biological systems, it is necessary to study the dispersion size of nanoparticles in different solutions [33]. Figure 4A, B shows that the BiF₃:Ln@PVP NPs have a relatively narrow distribution in DI and PBS (pH=7.4), indicating that the BiF₃:Ln@PVP NPs have

good stability in different solutions. Thus, they are suitable for biological applications.

The cytotoxicity of BiF₃:Ln@PVP NPs were studied after proving that BiF₃:Ln@PVP NPs have good stability in different solutions. The live-dead experiment evaluated the cytotoxicity of BiF₃:Ln@PVP NPs. No obvious red fluorescence was observed when the concentration of BiF₃:Ln@PVP NP suspension reached 400 µg/mL and was cultured with HepG2 cells for 24 h (compared with the control group; Fig. 4C). This indicates that there was no significant cell death in the experimental group. Subsequently, a CCK-8 assay was performed to further study the cytotoxicity of BiF₃:Ln@PVP NPs. Figure 4D shows the cell viability of HepG2 cells incubated with various concentrations of BiF₃:Ln@PVP NP suspensions for 24 h, the experimental groups of HepG2 cells all had relatively high cell viabilities. Furthermore, the cell viability was as high as 85.96% when the concentration of the BiF₃:Ln@PVP NP suspension reached to 400 µg/mL. These results demonstrated that the BiF₃:Ln@PVP NPs possessed favorable biocompatibility in vitro, which may be attributed to the coating of PVP on the surface of the BiF₃:Ln@PVP NPs.





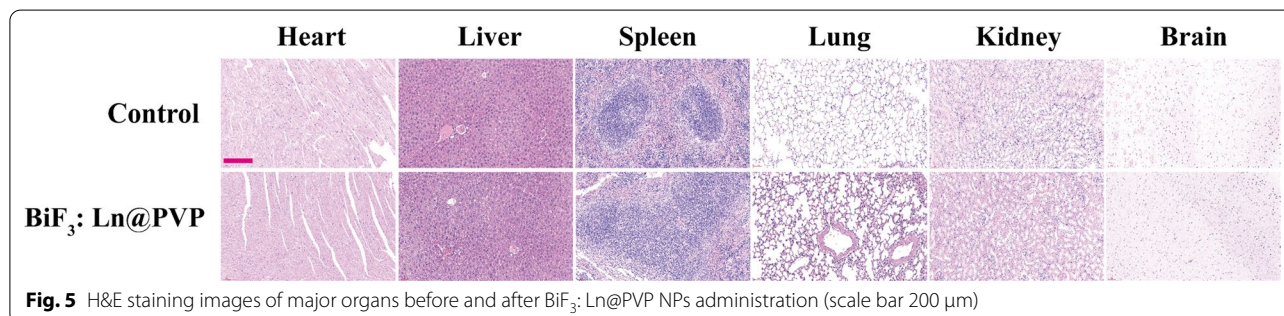
Biocompatibility of BiF₃: Ln@PVP NPs In Vivo

In addition to low cytotoxicity, good in vivo biocompatibility is another necessary condition for the clinical use of contrast agents [35]. Thus, the BiF₃: Ln@PVP NP suspension was prepared and injected into the mice at 200 mg/kg (100 µL) through the tail vein. The same volume of PBS solution was injected and set as the control group. After 24 h, the mice were sacrificed, and major organs were excised during necropsy. The H&E staining was performed to evaluate the system toxicity. Figure 5 shows no

obvious pathological abnormalities after BiF₃: Ln@PVP NPs administration for 24 h. These results indicate that BiF₃: Ln@PVP NPs have good biocompatibility, which is consistent with the low cytotoxicity shown above.

The Ability of BiF₃: Ln@PVP NPs In Vitro CT Imaging

Elements with high atomic numbers usually have high contrast effects because of their great X-ray attenuation. For example, contrast agents prepared from precious metals with a high atomic number (Au [36], Ag



[37], etc.) have excellent CT imaging effects as previously reported. Therefore, a promising type of contrast agent can be considered. However, their high cost limits their further clinical application. Bismuth has good biological safety and low cost, with great X-ray attenuation ability [38–41]. Herein, to evaluate the contrast agent effect of BiF₃: Ln@PVP NPs, we compared the X-ray attenuation ability of BiF₃: Ln@PVP NPs with the commercial contrast agent Iohexol solution in vitro. Figure 6A, B shows the corresponding CT images of BiF₃: Ln@PVP and Iohexol under different operating voltage (50 kV and 80 kV, respectively). Figure 6A, B indicates that the gray level of the image gradually changes from black shade to white shade as the concentration of the suspensions increased. However, at the same concentration, BiF₃: Ln@PVP has a brighter shade than Iohexol because the X-ray attenuation coefficient of Bi is higher I (Bi is 5.74 cm² kg⁻¹ and I is 1.94 cm² kg⁻¹ at 100 keV) [42].

Figure 6C shows that the CT value (Hounsfield Unit, HU) increases linearly with increasing BiF₃: Ln@PVP NPs and Iohexol concentration (both $R^2 > 0.99$) regardless of the operating voltage. The CT value of the unit mass concentration of BiF₃: Ln@PVP NPs is much higher than that of Iohexol (1.5- and 1.7-fold higher than that at 50 kV and 80 kV, respectively). These results indicate that the BiF₃: Ln@PVP NPs can provide better contrast effect at the same doses versus commercial Iohexol; these data confirm that the BiF₃: Ln@PVP NPs have good in vitro CT imaging capability, which is of great significance because it can reduce the amount of contrast agent while ensuring good imaging effects.

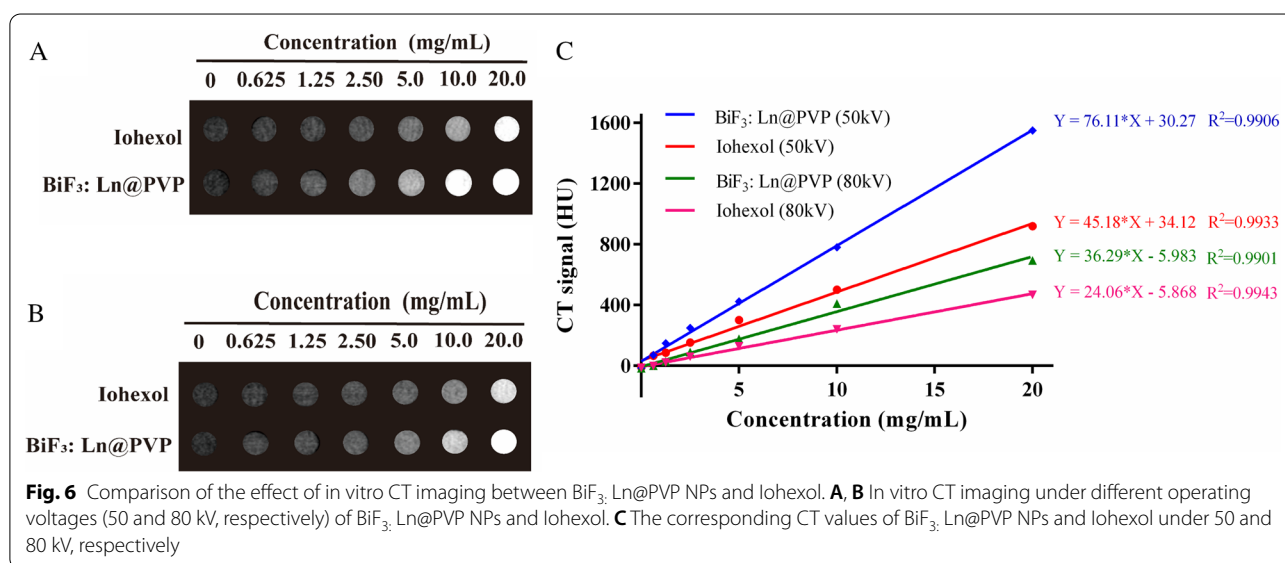
This can significantly reduce the toxicity and side effects.

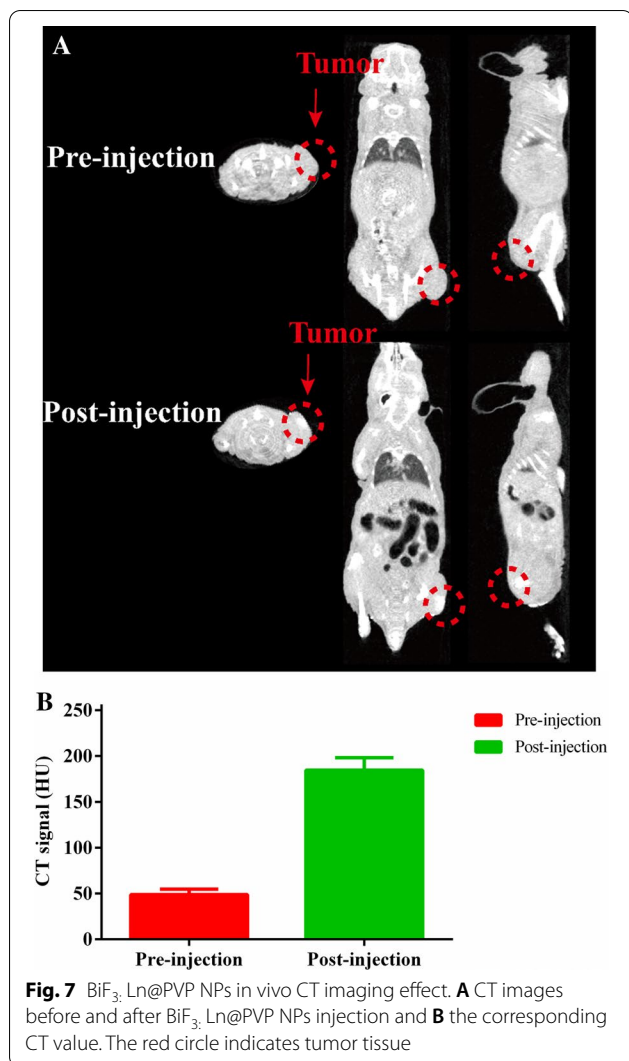
Contrast Effect of BiF₃: Ln@PVP NPs In Vivo CT Imaging

The BiF₃: Ln@PVP NP suspension was next injected intratumorally into the tumor-bearing mice (200 mg/kg, 100 μL) to evaluate the contrast effect of BiF₃: Ln@PVP NPs in vivo CT imaging. A strong signal intensity change is detected versus baseline in the same tumor area after 1 h administration of BiF₃: Ln@PVP NP suspension (Fig. 7A). Meanwhile, Fig. 7B shows that the CT value of post-injection (184.58 HU) is much higher than pre-injection (48.9 HU). This is due to the increase in the X-ray attenuation coefficient of tumor tissue after BiF₃: Ln@PVP NPs are distributed in tumor tissue. The results indicate that the BiF₃: Ln@PVP NPs have great in vivo CT imaging ability.

GI Tract CT Imaging Performance of BiF₃: Ln@PVP NPs and Its GI Toxicity

Encouraged by the promising results above, we were motivated to further evaluate potential application of BiF₃: Ln@PVP NPs in CT imaging. As a common non-invasive imaging method, CT plays a vital role in the diagnosis of GI diseases and the formulation of treatment plans due to its convenient image processing, no tissue damage, and painlessness of patients [43, 44]. The commonly used barium sulfate contrast agent is usually used together with aerogenic powder. Owing to the different densities produced by the two substances, the GI tract cannot always be clearly displayed resulting in missed diagnoses, which limit its in clinical use [45]. Thus, it is of great significance to explore high-efficiency GI contrast





agents that do not require additional assistance. In this work, we explored the effect of BiF₃: Ln@PVP NPs on the GI tract in nude mice.

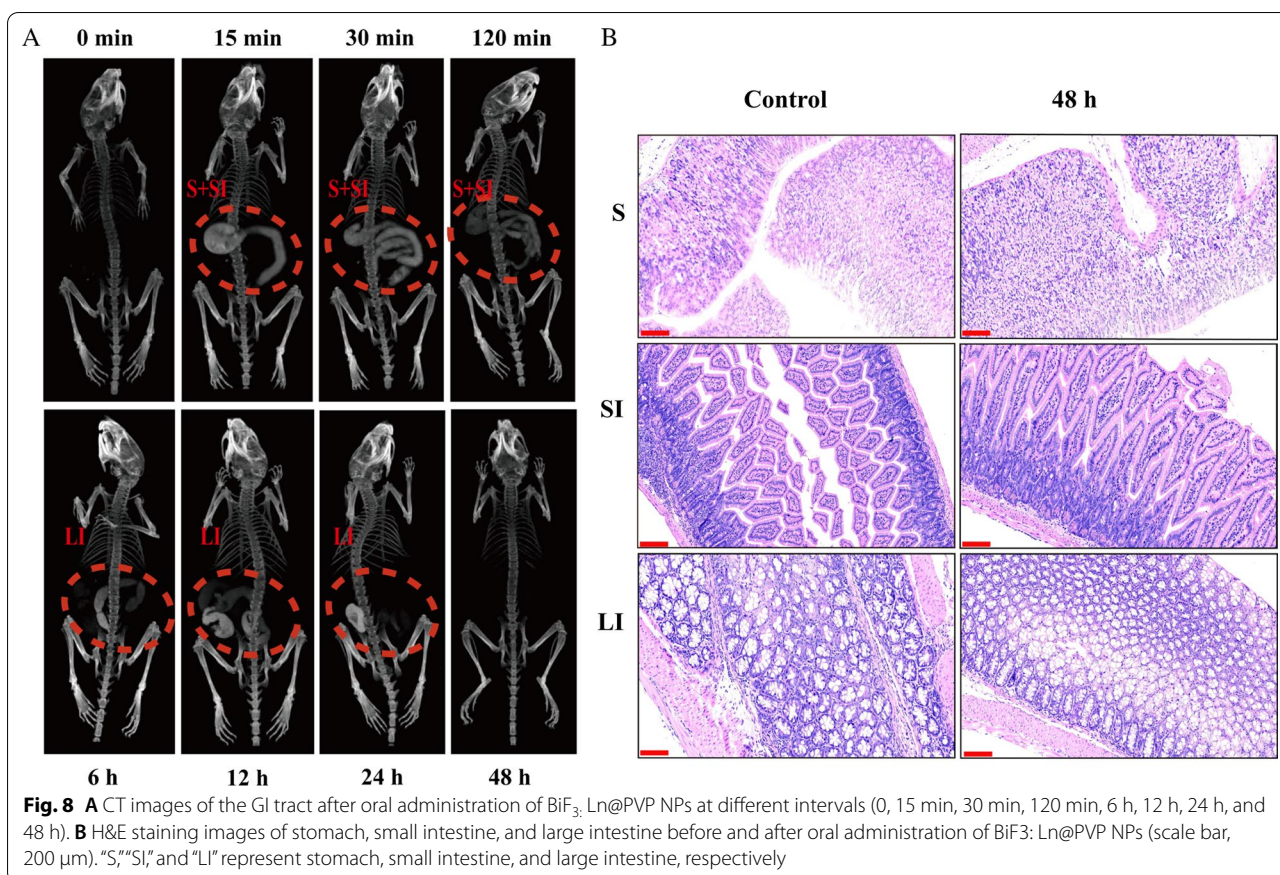
Figure 8A shows that the shape of the stomach and small intestine became visible after oral administration of BiF₃: Ln@PVP NP suspension (20 mg/mL, 300 μ L) for 15 min. At 30 min, the BiF₃: Ln@PVP NPs were metabolized with the peristalsis of the stomach. The stomach morphology became weakened. At 120 min, most of the BiF₃: Ln@PVP NPs were metabolized from the stomach, and only the remaining stomach outline was visible. The BiF₃: Ln@PVP NPs began to appear in the contour of the large intestine at 6 h, indicating that the nanoparticles began to become enriched in the large

intestine; the morphology of the large intestine was clearly visible at 12 h. Most of the BiF₃: Ln@PVP NPs were excreted and only a small part remains at 24 h. We could not observe the GI morphology at 48 h interval, indicating that all the BiF₃: Ln@PVP NPs were excreted from GI tract. After the nanoparticles were completely excreted from the GI tract, the mice were sacrificed and the stomach, small intestine and large intestine were removed for an H&E assay to evaluate the GI toxicity of the BiF₃: Ln@PVP NPs. Figure 8B shows no obvious histological changes in the stomach, small intestine, or large intestine after 48 h of oral administration of BiF₃: Ln@PVP NPs demonstrating that the BiF₃: Ln@PVP NPs have no significant toxicity to the GI tract. These results indicate that BiF₃: Ln@PVP NPs can be used as a potential CT contrast agent for the GI tract to enhance the CT imaging performance of the GI tract, while having no obvious toxicity to the GI tract.

These results indicate that BiF₃: Ln@PVP NPs have potential as clinical CT contrast agents for tumor and gastrointestinal imaging. However, owing to the limitation of particle size, BiF₃: Ln@PVP NPs cannot achieve good enhanced permeability and retention (EPR) effect [46]. The long-term biological safety of BiF₃: Ln@PVP NPs and the metabolic process in vivo requires further study.

Conclusion

Herein, we synthesized a novel CT contrast agent via hydrothermal process. The TEM data show that BiF₃: Ln@PVP NPs have a uniform spherical structure with a mean size of about 380 nm. The FTIR spectra show that the PVP was successfully wrapped on the surface of the nanoparticles to improve the biological safety of the nanoparticles. We then compared the in vitro CT imaging effect with Iohexol under different operating voltages. The results indicate that the BiF₃: Ln@PVP NPs have a better X-ray attenuation ability than Iohexol. Biocompatibility studies show that the BiF₃: Ln@PVP NPs have no obvious toxicity to major organs in vivo. Finally, the good X-ray attenuation ability allows BiF₃: Ln@PVP NPs to have good contrast imaging effects in vivo to successfully visualize the GI tract in detail without causing damage to the GI tract. Therefore, our work offers a high-efficiency CT contrast agent with good water-soluble stability, good biosafety, and high efficiency. These features make it a potential candidate for clinical contrast agents.



Abbreviations

CT: Computed tomography; PVP: Polyvinylpyrrolidone; GI: Gastrointestinal; PLAL: Pulsed laser ablation in liquid; Bi: Bismuth; Gd: Gadoliniumnitrate; Yb: Ytterbium; Er: Erbium; Au: Gold; Ta: Tantalum; Pt: Platinum; I: Iodine; NP: Nano-particle; CCK-8: Cell counting kit-8; RPMI: Roswell Park Memorial Institute; FBS: Fetal bovine serum; Ln: Lanthanides; DI: Deionized water; TEM: Transmission electron microscopy; EDS: Energy dispersive spectrum; FTIR: Fourier transform infrared spectroscopy; XRD: Powder X-ray diffraction; DLS: Dynamic light scattering; PI: Propidium iodide; H&E: Hematoxylin–eosin; HU: Hounsfield unit; EPR: Enhanced permeability and retention.

Acknowledgements

The authors would like to thank the Sabendong Nano Research Institute of Xiamen University for their help with the nanoparticles characterization section.

Authors' contributions

Y.Q.C, J.H.Y and F.H.L proposed the ideas. J.X and Z.L.Z completed the experiment and original draft writing. J.H.Y and F.H.L reviewed and edited the original draft. S.H.M. and S.Y.W together carried out with the in vivo experiment part. X.L and J.J.L assisted in date collection and statistical analysis. This article has been read by all authors and agreed to be published.

Funding

We thank the National Natural Science Foundation of China (Grant Number: 81773770) and Science and Technology Department of Fujian Province (Grant Numbers: 2018R1036-1, 2019R1001-2 and 2020R1001001.) for their financial support for this research.

Availability of data and materials

The datasets used and/or analyzed during the current study are available from the corresponding author on reasonable request.

Declaration

Competing interests

All authors indicate that they have no conflict of interest.

Author details

¹Cancer Research Center, Medical College, Xiamen University, Xiamen 361102, China. ²College of Energy, Xiamen University, Xiamen 361102, China. ³The 174th Clinical College of People's Liberation Army, Anhui Medical University, Hefei 230032, China.

Received: 15 April 2021 Accepted: 10 August 2021

Published online: 14 August 2021

References

- Lusic H, Grinstaff MW (2013) X-ray-computed tomography contrast agents. *Chem Rev* 113(3):1641–1666
- Lee N, Choi SH, Hyeon T (2013) Nano-sized CT contrast agents. *Adv Mater* 25(19):2641–2660
- Ardila D, Kiraly AP, Bharadwaj S et al (2019) End-to-end lung cancer screening with three-dimensional deep learning on low-dose chest computed tomography. *Nat Med* 25(6):954–961
- Tierney WM, Kochman ML, Scheiman JM (2005) Computed tomography versus endoscopic ultrasonography for staging of pancreatic cancer. *Ann Intern Med* 142(7):590 (author reply 590–591)
- Segal E, Sirlin CB, Ooi C et al (2007) Decoding global gene expression programs in liver cancer by noninvasive imaging. *Nat Biotechnol* 25(6):675–680

6. Jemaa Y, Houissa F, Trabelsi S et al (2008) Endoscopic ultrasonography versus helical CT in diagnosis and staging of pancreatic cancer. *Tunis Med* 86(4):346–349
7. Fu JJ, Guo JJ, Qin AP et al (2020) Bismuth chelate as a contrast agent for X-ray computed tomography. *J Nanobiotechnol* 18(1):1–10
8. Maurer T, Souvatzoglou M, Kubler H et al (2012) Diagnostic efficacy of [^{11}C]choline positron emission tomography/computed tomography compared with conventional computed tomography in lymph node staging of patients with bladder cancer prior to radical cystectomy. *Eur Urol* 61(5):1031–1038
9. Liao WH, Lei P, Pan JB et al (2019) Bi-DTPA as a high-performance CT contrast agent for in vivo imaging. *Biomaterials* 203:1–11
10. Morcos SK, Thomsen HS (2001) Adverse reactions to iodinated contrast media. *Eur Radiol* 11(7):1267–1275
11. Hunt CH, Hartman RP, Hesley GK (2009) Frequency and severity of adverse effects of iodinated and gadolinium contrast materials: retrospective review of 456,930 doses. *Am J Roentgenol* 193(4):1124–1127
12. Oh MH, Lee N, Kim H et al (2011) Large-scale synthesis of bioinert tantalum oxide nanoparticles for x-ray computed tomography imaging and bimodal image-guided sentinel lymph node mapping. *J Am Chem Soc* 133(14):5508–5515
13. Jokest JV, Gambhir SS (2011) Molecular imaging with theranostic nanoparticles. *Acc Chem Res* 44(10):1050–1060
14. Liu YL, Ai KL, Lu LH (2012) Nanoparticulate X-ray computed tomography contrast agents: from design validation to in vivo applications. *Acc Chem Res* 45(10):1817–1827
15. Popovtzer R, Agrawal A, Kotov NA et al (2008) Targeted gold nanoparticles enable molecular CT imaging of cancer. *Nano Lett* 8(12):4593–4596
16. Balati A, Bazilio A, Shahriar A et al (2019) Simultaneous formation of ultra-thin MoSe_2 nanosheets, inorganic fullerene-like MoSe_2 and MoO_3 quantum dots using fast and ecofriendly pulsed laser ablation in liquid followed by microwave treatment. *Mater Sci Semicond Process* 99:68–77
17. Balati A, Tek S, Nash K et al (2019) Nanoarchitecture of TiO_2 microspheres with expanded lattice interlayers and its heterojunction to the laser modified black TiO_2 using pulsed laser ablation in liquid with improved photocatalytic performance under visible light irradiation. *J Colloid Interface Sci* 541:234–248
18. Balati A, Wagle D, Nash KL et al (2018) Heterojunction of TiO_2 nanoparticle embedded into ZSM5 to 2D and 3D layered-structures of MoS_2 nanosheets fabricated by pulsed laser ablation and microwave technique in deionized water: structurally enhanced photocatalytic performance. *Appl Nanosci* 9(1):19–32
19. Liu Y, Liu C, Shi C et al (2021) Carbon-based quantum dots (QDs) modified ms/tz-BiVO $_4$ heterojunction with enhanced photocatalytic performance for water purification. *J Alloys Compd* 881:160437
20. Ma L, Fan H, Fu K et al (2017) Protonation of graphitic carbon nitride ($\text{g-C}_3\text{N}_4$) for an electrostatically self-assembling carbon@ $\text{g-C}_3\text{N}_4$ core-shell nanostructure toward high hydrogen evolution. *ACS Sustain Chem Eng* 5(8):7093–7103
21. Tian H, Fan H, Ma J et al (2018) Pt-decorated zinc oxide nanorod arrays with graphitic carbon nitride nanosheets for highly efficient dual-functional gas sensing. *J Hazard Mater* 341:102–111
22. Balati A, Matta A, Nash K et al (2020) Heterojunction of vertically aligned MoS_2 layers to Hydrogenated Black TiO_2 and rutile based inorganic hollow microspheres for the highly enhanced visible light arsenic photooxidation. *Compos Part B Eng* 185:107785
23. Xu C, Wang Y, Zhang C et al (2017) AuGd integrated nanoprobe for optical/MRI/CT triple-modal in vivo tumor imaging. *Nanoscale* 9(13):4620–4628
24. Jin Y, Ma X, Zhang S et al (2017) A tantalum oxide-based core/shell nanoparticle for triple-modality image-guided chemo-thermal synergetic therapy of esophageal carcinoma. *Cancer Lett* 397:61–71
25. Yu C, Eustaquio N, Calello DP et al (2019) Bismuth subsalicylate coagulation in a patient with chronic liver disease. *J Med Toxicol* 15(3):198–201
26. Naha PC, Al Zaki A, Hecht E et al (2014) Dextran coated bismuth-iron oxide nanohybrid contrast agents for computed tomography and magnetic resonance imaging. *J Mater Chem B* 2(46):8239–8248
27. Du FY, Lou JM, Jiang R et al (2017) Hyaluronic acid-functionalized bismuth oxide nanoparticles for computed tomography imaging-guided radiotherapy of tumor. *Int J Nanomed* 12:5973–5992
28. Chen J, Yang XQ, Qin MY et al (2015) Hybrid nanoprobe of bismuth sulfide nanoparticles and CdSe/ZnS quantum dots for mouse computed tomography/fluorescence dual mode imaging. *J Nanobiotechnol* 13:76
29. Mahvi M, Delavari HH, Poursalehi R (2018) Rapid microwave-assisted synthesis of Bi_2Te_3 nanoflakes as an efficient contrast agent for X-ray computed tomography. *Ceram Int* 44(8):9679–9683
30. Fang Y, Peng C, Guo R et al (2013) Dendrimer-stabilized bismuth sulfide nanoparticles: synthesis, characterization, and potential computed tomography imaging applications. *Analyst* 138(11):3172–3180
31. Hernandez-Rivera M, Kumar I, Cho SY et al (2017) High-performance hybrid bismuth-carbon nanotube based contrast agent for X-ray CT imaging. *ACS Appl Mater Interfaces* 9(7):5709–5716
32. Curcio A, Silva AKA, Cabana S et al (2019) Iron oxide nanoflowers @ CuS hybrids for cancer tri-therapy: interplay of photothermal therapy, magnetic hyperthermia and photodynamic therapy. *Theranostics* 9(5):1288–1302
33. Li Y, Shaker K, Svenda M et al (2020) Synthesis and cytotoxicity studies on Ru and Rh nanoparticles as potential X-ray fluorescence computed tomography (XFCT) contrast agents. *Nanomater Basel* 10(2):310
34. Soltani N, Saion E, Erfani M et al (2012) Influence of the polyvinyl pyrrolidone concentration on particle size and dispersion of ZnS nanoparticles synthesized by microwave irradiation. *Int J Mol Sci* 13(10):12412–12427
35. Jeon M, Halbert MV, Stephen ZR et al (2020) Iron oxide nanoparticles as T1 contrast agents for magnetic resonance imaging: fundamentals, challenges, applications, and prospectives. *Adv Mater* 33:e1906539
36. Aouidat F, Boumati S, Khan M et al (2019) Design and synthesis of gold-gadolinium-core-shell nanoparticles as contrast agent: a smart way to future nanomaterials for nanomedicine applications. *Int J Nanomed* 14:9309–9324
37. Caro C, Dalmases M, Figuerola A et al (2017) Highly water-stable rare ternary Ag–Au–Se nanocomposites as long blood circulation time X-ray computed tomography contrast agents. *Nanoscale* 9(21):7242–7251
38. Liu Y, Ai K, Liu J et al (2012) Hybrid BaYbF $_5$ nanoparticles: novel binary contrast agent for high-resolution in vivo X-ray computed tomography angiography. *Adv Healthc Mater* 1(4):461–466
39. Ai K, Liu Y, Liu J et al (2011) Large-scale synthesis of Bi(2)S(3) nanodots as a contrast agent for in vivo X-ray computed tomography imaging. *Adv Mater* 23(42):4886–4891
40. Yu SB, Watson AD (1999) Metal-based X-ray contrast media. *Chem Rev* 99(9):2353–2378
41. Lei PP, Zhang P, Yuan QH et al (2015) $\text{Yb}^{3+}/\text{Er}^{3+}$ -codoped Bi_2O_3 nanoparticles: probe for upconversion luminescence imaging and binary contrast agent for computed tomography imaging. *ACS Appl Mater Interfaces* 7(47):26346–26354
42. Kim D, Park S, Lee JH et al (2007) Antibiofouling polymer-coated gold nanoparticles as a contrast agent for in vivo X-ray computed tomography imaging. *J Am Chem Soc* 129(41):12585–12585
43. Jelicks LA (2010) Imaging the gastrointestinal tract of small animals. *J Neuroparasitol* 1:N100504
44. Liu Z, Ju E, Liu J et al (2013) Direct visualization of gastrointestinal tract with lanthanide-doped BaYbF $_5$ upconversion nanoprobe. *Biomaterials* 34(30):7444–7452
45. Peterson CM, Anderson JS, Hara AK et al (2009) Volvulus of the gastrointestinal tract: appearances at multimodality imaging. *Radiographics* 29(5):1281–1293
46. Cheng X, Li H, Ge X et al (2020) Tumor-microenvironment-responsive size-shrinkable drug-delivery nanosystems for deepened penetration into tumors. *Front Mol Biosci* 7:576420

Publisher's Note

Springer Nature remains neutral with regard to jurisdictional claims in published maps and institutional affiliations.